
Investigation of the Flow Randomization Process in a Transitional Boundary Layer

Daniel Meyer, Ulrich Rist, and Markus Kloker

Institut für Aerodynamik und Gasdynamik, Universität Stuttgart, Pfaffenwaldring
21, D-70550 Stuttgart, Germany, e-mail: [name]@iag.uni-stuttgart.de

This work is devoted to the investigation of the late stages of the laminar-turbulent transition process in a flat-plate boundary layer without pressure gradient. Similar to a turbulent boundary layer these stages are dominated by nonlinear flow dynamics and by the occurrence of coherent vortex motions in the boundary layer, which are far from being well understood, up to now. The work consists of two parts: a description of some salient features of the numerical method, and an account of some specific results of a numerical study of the flow randomization process in K-type transition that has been performed conjointly with a wind-tunnel investigation at the Technical University of Berlin.

1 Introduction

The different aspects of laminar-turbulent transition have been subject of intensive research for the past few years, especially in Germany where a national research program has been established in 1996 by the DFG [12]. From a better understanding of transition, improvements in its prediction, new means for flow control, and basic contributions to turbulence research can be expected. In addition to performing various kinds of laboratory or free-flight experiments, direct numerical simulation has become a reliable tool to perform “virtual experiments” under carefully controlled boundary conditions which allow to trace down several observations to their physical origins. The focus of the present work is on the late stages of the transition process, which are dominated by nonlinear flow dynamics and by the occurrence of coherent vortex motion in the boundary layer. In contrast to the earlier stages of the transition process that can be adequately described by linear (primary) and secondary stability theory, these are not as well understood and their numerical simulation demands large computer resources, despite the use of adapted and optimized numerical algorithms.

2 Numerical method

The well-proven numerical method is based on a velocity-vorticity formulation of the Navier-Stokes equations for an incompressible fluid. The so-called spatial model is applied, where all three spatial dimensions and time are discretized without any modeling assumptions for a spatially growing boundary layer. For the present simulations, the flow is split into a steady two-dimensional baseflow and an unsteady three-dimensional disturbance flow. The baseflow has to be calculated separately before the equations for the disturbance flow field can be solved. In this model the nonlinear meanflow deformation is obtained as the temporal mean of the fluctuating disturbance quantities at any given point in the flow field. Since the flow can be considered periodic in spanwise direction, a Fourier ansatz in this direction is used, and the equations and boundary conditions are transformed accordingly. The nonlinear terms are solved using a pseudo-spectral technique introduced by [10] which ensures an aliasing-free computation of all spanwise modes. High-order compact finite differences are used for discretization of the wall-normal and the downstream direction. Explicit time integration is performed by a standard Runge-Kutta scheme of 4th-order accuracy. A scheme of alternating high-order up- and downwind-biased compact finite differences is used in subsequent intermediate Runge-Kutta steps for computation of the streamwise derivatives of the nonlinear terms. This method leads to a finite-difference scheme with the dispersion characteristics of a central scheme, but, in addition, provides the appropriate amount of numerical damping for possibly occurring high-wavenumber modes on the used grid.

The disturbances in the DNS are generated by suction and blowing within a disturbance strip at the wall. Shortly upstream of the outflow boundary the disturbance vorticity vector is forced to zero in a buffer domain to prevent undue reflections induced otherwise by large-amplitude disturbances passing through. The numerical method has been extensively verified (checked for consistent discretization and convergence) and validated (compared with linear stability theory and experimental data) and has proven to be a useful research tool (cf. [12]).

Due to the extraordinary performance requirements of spatial direct numerical simulations we strongly depend on high processing speed on a single CPU. This can usually only be provided by vector-type processors. Therefore, our code is especially prepared to take maximum advantage of such CPUs by providing simple, well vectorizable, high work-load algorithmic loops. However, to decrease the turn around-time further we apply two fundamentally different parallelization techniques at the same time. A hybrid approach, using directive-based shared-memory parallelization with OpenMP and explicitly coded distributed-memory parallelization with MPI, allows for efficient use of state-of-the-art multi-node supercomputers with multiple CPUs per node. We combine classical domain decomposition in physical space with parallel computation of the temporally decoupled spanwise Fourier modes in spec-

tral space in our code. A sketch of our parallelization strategy is given in figure 1, showing, as a simple example, a run with two MPI processes and three OpenMP threads running in each MPI process, i.e. using a total of 6 CPUs. As long as we are in physical space (upper part of figure 1), we use domain decomposition for the MPI processes by dividing the downstream direction into as many equally sized regions as MPI processes are available. The wall-normal direction will be worked on in parallel by the different OpenMP threads in each MPI process, because all computations in that direction can be performed independently of each other. When in spectral space (lower part of figure 1), the number of Fourier modes is divided by the number of MPI processes and each MPI process is responsible for his share of consecutive Fourier modes. Within the MPI process the OpenMP threads work on different Fourier modes in parallel, because the computations for different modes are independent of each other. During the computation data have to be exchanged between both arrangements in order to compute the non-linear product terms of the Navier-Stokes equations in physical space. These terms provide the coupling between the different Fourier modes. The data exchange between the two different arrangements of data in memory is done by a call to the MPI subroutine `MPI_ALLTOALL` because every MPI process must exchange data with all other MPI processes. Since MPI only provides facilities to exchange data stored in linear buffers in memory (consecutive regions in memory), a quite elaborate data sorting is required in order to write into or read from these linear buffers. The involved three-dimensional arrays used for data storage in memory have different dimension sizes for both data arrangements, which also contributes to a tedious sorting process.

The performance on the NEC-SX/5 is about 2 GFlops per CPU for the whole code, which corresponds to roughly 50% of the theoretical peak performance. In single subroutines a performance of up to 3.8 GFlops is achieved. Our code seems to be bandwidth limited, because on the NEC-SX/4 we achieve about 60% of the theoretical peak performance, which is most likely due to the fact that the NEC-SX/4 has a faster memory interface (relative to the available CPU performance on that machine). The code scales very well in shared-memory environments up to about 12 CPUs using OpenMP directives. For larger numbers of parallel CPUs the computations should be distributed on more than one node using the MPI parallelization additionally. Using MPI within the same node is not desirable, because of the overhead generated by the data exchange required between the MPI processes. Up to now, we have used the code on the Cray-T3E with up to 230 CPUs in parallel (using MPI), and we did successful test runs on two NEC-SX/5 nodes during maintenance times with our hybrid approach as described above. However, up to now production runs have always been done on a single NEC-SX/5 node using a maximum of 14 CPUs.

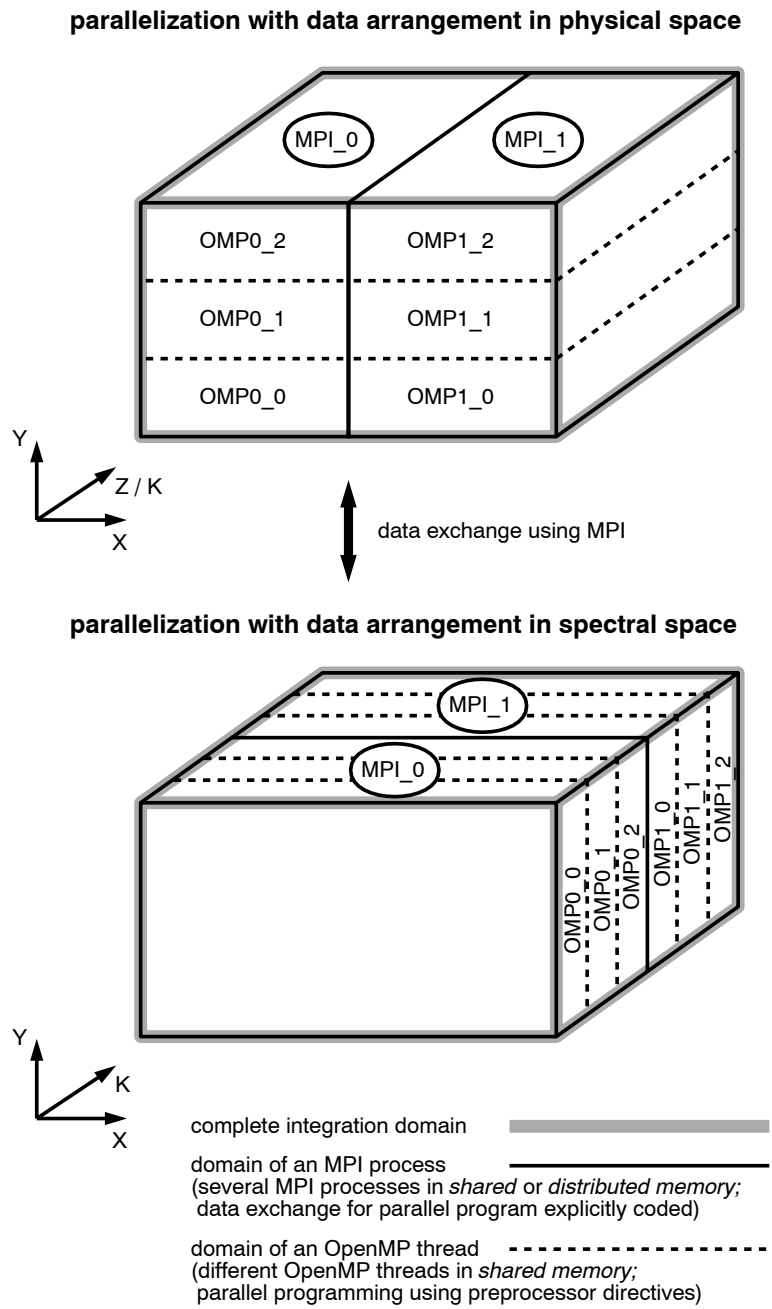


Fig. 1. Sketch of strategy for the hybrid parallelization approach using OpenMP and MPI at the same time

3 Results

In the HLRS-project “LAMTUR” a considerable number of investigations related to laminar-turbulent transition have been performed recently, ranging from the reception of initial disturbances from the free-stream flow into the boundary layer [15] to investigations of the late stages of the transition process [3, 7, 13]. Only the last of these problems will be presented here. For more references see [4, 6, 11, 12, 14]).

For a mutual verification and for gaining additional insights wind-tunnel experiments have been performed at the Hermann-Föttinger-Institute of the Technical University of Berlin in parallel to the present numerical simulations for a corresponding set-up. More information about the experiment can be found in [1] together with several direct quantitative comparisons between simulations and experiment. A sketch of the numerical integration domain related to the experimental set-up is given in figure 2 and the parameters of the simulation are summarized in table 1. All downstream positions are given in experimental coordinates.

Time-wise periodic suction and blowing with a disturbance frequency of 62.5 Hz is applied within a disturbance strip at the wall located at $x = 550$ mm which corresponds to a local Reynolds number (based on the displacement thickness) of $Re_{\delta_1} = 730$. The disturbance input consists of a large-amplitude two-dimensional disturbance (a so-called Tollmien-Schlichting wave) and a number of spanwise periodic disturbances which sum up to a peak amplitude in the spanwise centre of the integration domain at $z = 0$ that mimics the disturbances produced in the experiment by a series of loudspeakers (see Bake *et al.* [1]). However, it turned out that the amplitudes of the timewise periodic disturbance had to be quite large right from the very beginning in order to trigger the transition process within a short distance downstream of their source. Therefore, nonlinear wave-interactions are already important at the first data acquisition point of the experiment which is located at $x = 640$ mm. Iterative adjustments of the amplitudes of the periodic disturbances at the disturbance strip in the DNS were necessary in order to get a good overall agreement with the experimental measurements. This did not only lead to a close agreement

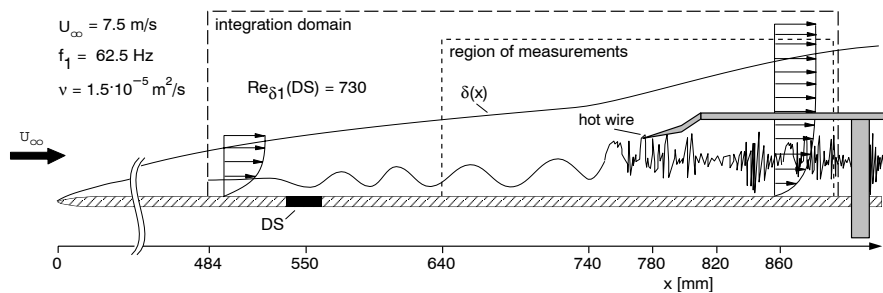


Fig. 2. Sketch of the integration domain

integration domain in mm ($X \times Y \times Z$)	$541.53 \times 18.48 \times 80.00$
grid points in x - and y -direction ($N \times M$)	2266×361
grid points within the wall zone	33
spectral modes ($K + 1$) (de-aliased)	154
grid points per wave length in z -direction (for the computation of non-linear terms)	512
number of unknowns (de-aliased)	$\approx 125 \cdot 10^6$
approximate number of grid points per disturbance wave length	180
resolution in mm ($\Delta x \times \Delta y$ (wall zone) $\times \Delta z$)	$0.2391 \times 0.0537(0.0269) \times 0.2614$
resolution in wall units at $x = 900$ mm ($\Delta x^+ \times \Delta y^+ \times \Delta z^+$)	$\approx 7.2 \times 0.8 \times 7.8$
non-dimensional circular disturbance frequency	$\beta = 10.472$
time step	$\Delta t = 1.067 \cdot 10^{-5}$ s
time steps per disturbance cycle	1500
non-dimensional wave number in x -direction	$\alpha = 29.2$
non-dimensional wave number in z -direction	$\gamma = 15.708$
reference values for normalization	$U_\infty = 7.5 \frac{m}{s}$, $L = 200$ mm $\nu = 1.5 \cdot 10^{-5} \frac{m^2}{s}$
number of disturbed spectral modes	21

Table 1. Simulation parameters

for the disturbance velocity-profiles in wall-normal and spanwise direction at the first measurement position, but also for the development of the disturbance amplitudes over the whole transition process (see [1]). All numerical results have been checked by grid refinement tests using partially a higher resolution than shown in table 1. During these tests, the wall-normal direction turned out to be the most critical one in terms of resolution requirements.

Since turbulent flow is by definition connected with random fluctuations with respect to the time- or (in our case) the phase-averaged flow, the question arises where these random fluctuations occur for the first time in a predominantly periodical flow, and by which mechanism they are amplified. Obviously, there must be a connection between the instability mechanisms and the structures inherent to the flow and the small-amplitude random background disturbances which are always present in real flow situations.

In the following, our observations concerning the flow randomization process in a transitional boundary layer without pressure gradient will be summarized. Additional details can be found in [1, 7, 8]. For the case with adverse pressure gradient see [5]. Here, we will focus on the flow structures which become only available via DNS, an appropriate post-processing, and flow visualizations. It will be shown that the flow randomization process can be understood by taking into account the development of the vortical structures

in the transitional boundary layer. However, apart from becoming increasingly smaller and more and more entangled with each other during the transition process, these structures are always closely related to high-shear layers inside the boundary layer. This is illustrated in figure 3 which is obtained in the so-called “two-spike stage”, i.e. at a spatial position where two subsequent highly characteristic velocity defects in the time signal at the edge of the boundary layer can be detected per disturbance cycle. These low-velocity regions mark the passage of small Ω -shaped vortex loops which can be seen in figure 3 between $x = 780$ and 800 mm. It turns out that high-shear layers are a by-product of the activity of the vortices embedded in the boundary layer. For instance, the legs of the characteristic so-called Λ -vortex in the left part of the figure rotate in such a way that they move low-speed fluid away from the wall in between them, while high-speed fluid is transported towards the wall on their outward sides. These two effects cause the high-shear layer on the inner top of the vortex and the outer bottom, respectively. At the ‘neck’ of the Λ -vortex at $x \approx 770$ mm, we find a strong upward movement of fluid in between the vortex’ legs due to induction by their counter rotation. This transport of low speed fluid away from the wall generates a high-shear layer above the vortex. Interestingly, the high-shear layer located on top of the Λ -structure from the previous disturbance cycle (i.e. the one further downstream) is always connected to the wall shear layer at the end of the next one. By this, structures from different disturbance cycles interact with each other. This is the beginning of a complicated process whose continuation will be shown and discussed below.

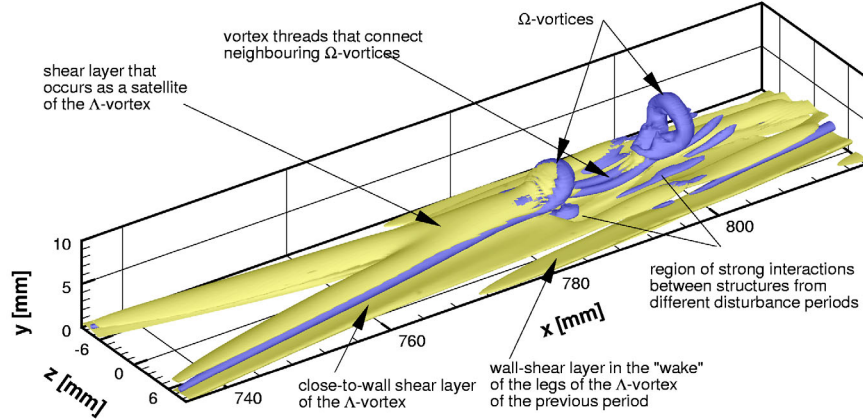


Fig. 3. Comparison of shear layers (yellow) and vortices (blue) inside the transitional boundary layer

The first random fluctuations occur at the tip of the A -vortex, where the ring-like Ω -vortices are formed. This formation process is very sensitive to background perturbations, as was also observed in turbulent channel flow by [16]. The formation and detachment of the Ω -vortex is accompanied by strong vortex stretching when the developing vortex lifts up in the boundary layer where it is accelerated. The stretching leads to increased fluid motion by induction, and, therefore, to a region of extremely high shear slightly above the stretched vortex legs. This shear layer disappears when the Ω -vortex detaches from the tip of the A -vortex and the legs, still connecting it with the A 's tip, start moving towards the wall. The sensitivity of the process of formation of the Ω -vortices to small random background perturbations is responsible for a slightly varying occurrence of the Ω -vortices in space and time from one cycle to another. These variations are perceived in the experiment as phase jitter and small amplitude variations of the spike signals. Since the fluid region around the Ω -vortices is a region of strong local velocity gradients, small-amplitude background perturbations will be amplified at these locations. Therefore, the amplified random motions will still be connected to the periodically occurring events in the flow, i.e. they will be strongest in regions where the local flow structures generate the largest gradients; they are no longer completely independent background perturbations. Such a correlation is actually found in the DNS as can be seen in figure 4 which shows a superposition of the non-periodic (i.e. random) fluctuations versus time together with the phase-averaged disturbance field in a crosscut at constant x . The same distribution of the random fluctuations has also been observed in the experiment (see [1]). Note: In the experiment it is easier to measure time signals for constant x versus time than to measure at several x -position at the same time (or phase) instant. The amplitude level of these random perturbations strongly depends on the amplitude level of the background disturbances at the inflow.

Once formed, the Ω -vortices have a strong effect on the surrounding fluid, especially down to the region close to the wall as already presented by Borodulin *et al.* [2]. Positive velocity fluctuations that move with the same speed as the Ω -vortices but much closer to the wall are observed in planes at $z \approx \pm 2$ mm. This influence can also be clearly observed in animations of $\partial U / \partial y$ at the wall produced from DNS data (not shown here). The modulation patterns of the wall values can be clearly attributed to the Ω -vortices in the outer part of the boundary layer because both move with the same velocity, which is almost free-stream speed. This way, the random motion in the outer part of the boundary layer is transferred to the region close to the wall where strong mean velocity gradients occur and the non-periodic fluctuations are amplified.

Another important effect of the vortices on the surrounding flow becomes apparent when we consider the instantaneous pressure field generated by the A -vortex in the boundary layer. This is shown in figure 5 with the help of two cuts through the pressure field in the plane $z = 0$ mm, and at the wall, respec-

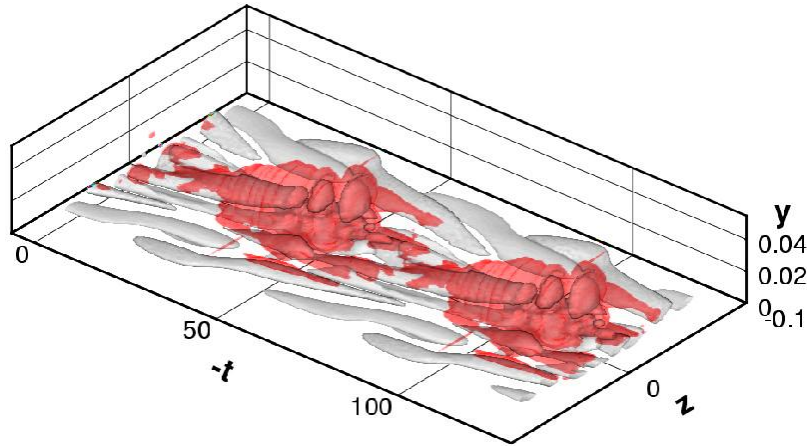


Fig. 4. Comparison of non-periodic fluctuations (red) with iso-surfaces of instantaneous disturbance velocity (grey) at $x = 780$ mm. Data computed from 6 disturbance cycles of a DNS with additional random background perturbations

tively. Because of the low pressure regions present within the vortex core, and at the locations where very strong induction occurs, pressure gradients are also generated at the wall. Such pressure gradients influence the production process of new vorticity at the wall. Therefore, the evolution of the coherent structures in the outer part of the boundary layer will directly influence the vorticity production at the surface of the flat plate. The pressure gradients may not be as pronounced in the ensuing turbulent boundary layer because of the huge number of structures in the flow, but for this stage of the flow development they seem to be relevant.

Thus, it turns out that the vortices and their residing high-shear layers are the main elements for a qualitative (and quantitative) description of the transition process. Their downstream development and their evolution towards a fully developed turbulent flow will be discussed now in connection with figures 6 and 7 at five phases of one disturbance cycle.

In figure 6, we can observe many Ω -vortices which evolve continuously at the tip of the Λ -structures. Despite the durability of these vortices in the outer part of the boundary layer, their initial formation seems to be very sensitive to small perturbations as already said above. Consequently, their streamwise distance with respect to each other varies slightly from one disturbance cycle to the next. The re-connections that are generated between the legs of the Λ -vortex, out of which the Ω -vortices emerge, must obviously be created by a viscous process because vortex lines are reconnecting at this stage of the development which cannot be explained by a purely inviscid mechanism. The subsequent detachment of the vortex loops from the tip of the Λ -vortex is a predominantly inviscid process, basically due to self-induction of the deformed

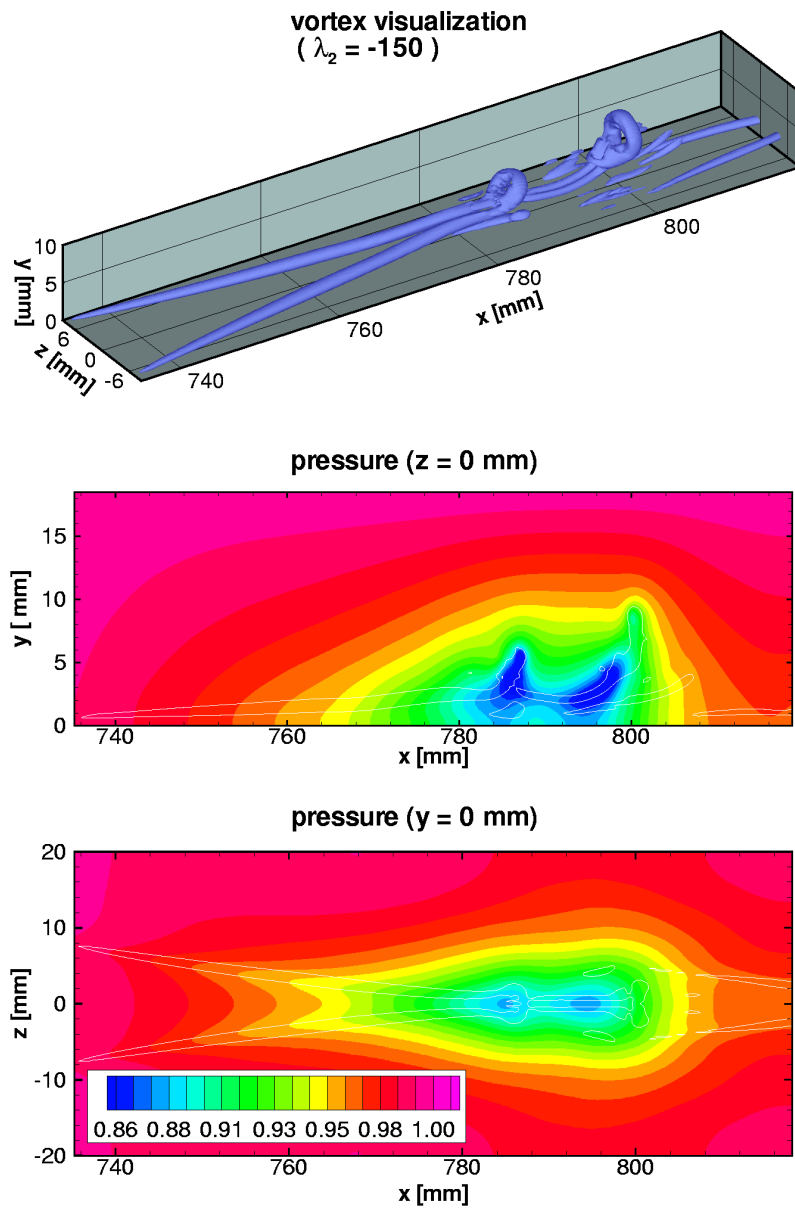


Fig. 5. Comparison of vortex visualization with the instantaneous pressure in the symmetry plane $z = 0$ and at the wall $y = 0$

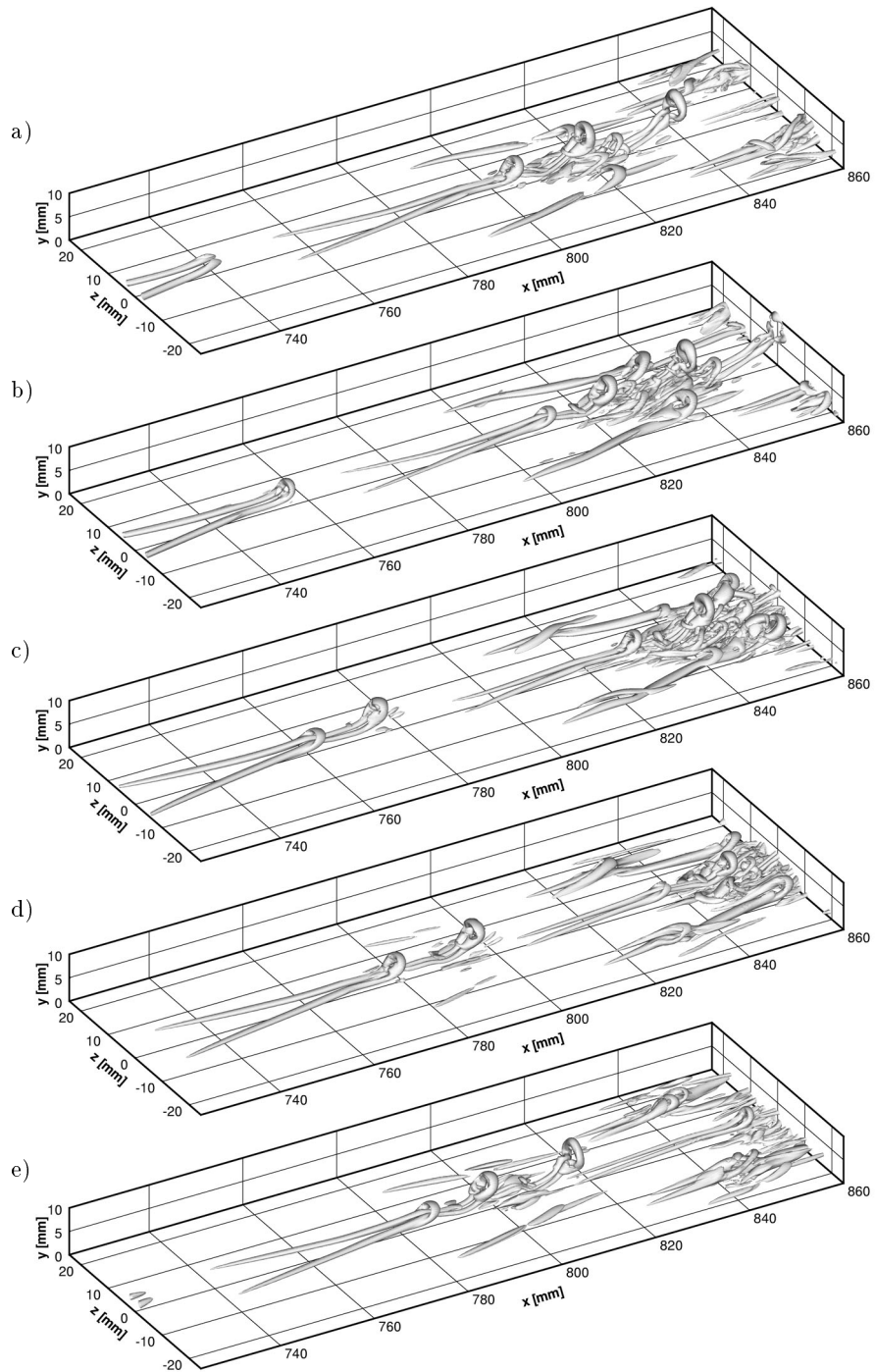


Fig. 6. Vortex visualization at five phases within one disturbance cycle; a) $t/T = 0.2$; b) $t/T = 0.4$; c) $t/T = 0.6$; d) $t/T = 0.8$; e) $t/T = 1$. Iso value $\lambda_2 = -150$

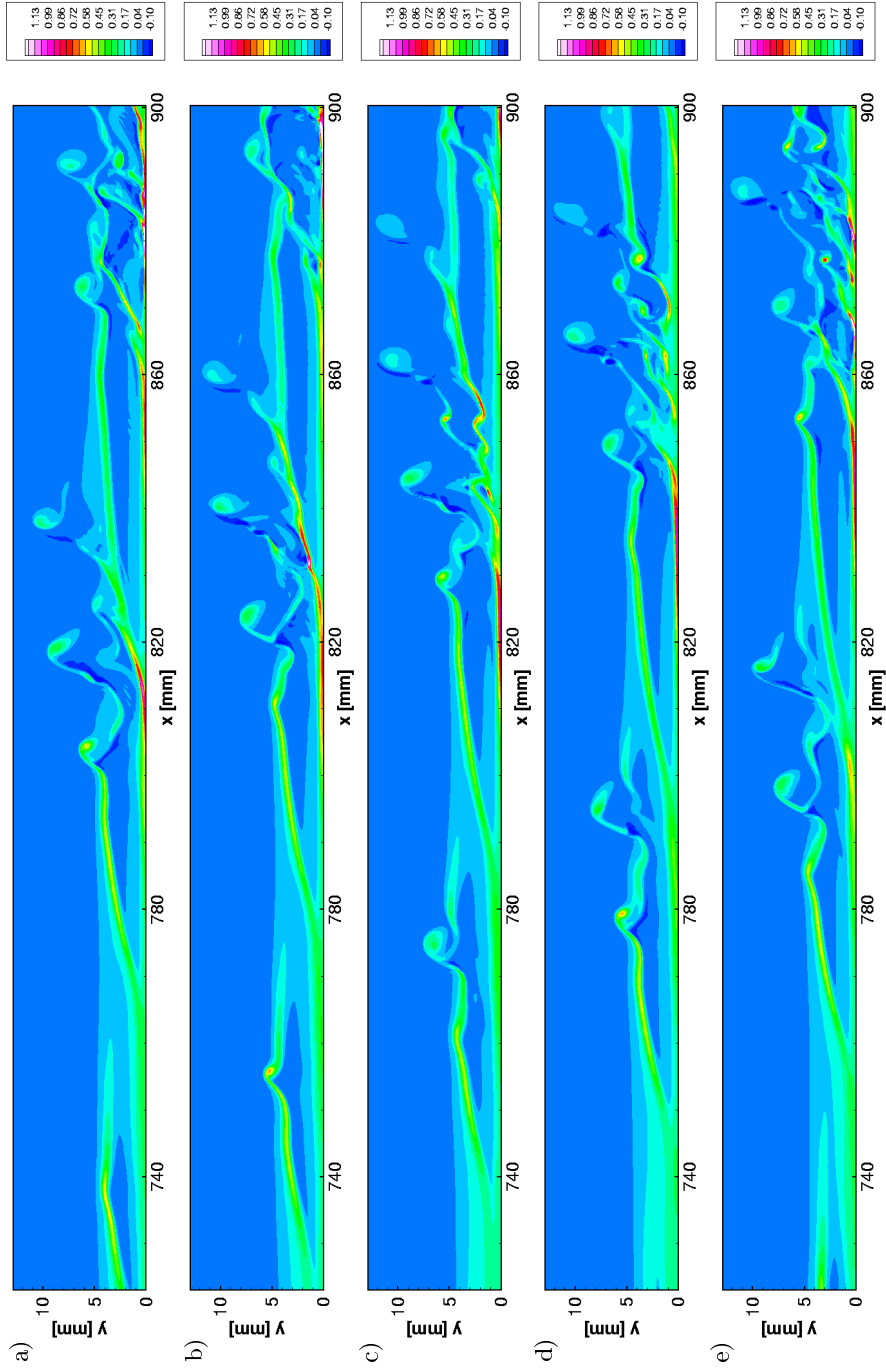


Fig. 7. Vorticity Ω_z at $z = 0$ mm for five consecutive instants from $t/T = 0.2$ to $t/T = 1$ (from left to right) as in fig. 6. $\Omega_z = \frac{\partial U}{\partial y} - \frac{\partial V}{\partial x}$

vortex line moving in the mean shear, as suggested in the work of Moin, Leonard und Kim [9].

Between any two Ω -vortices that were originally generated at the tip of the A -vortex and already have left the tip, there is only a relatively weak shear layer visible in figure 7. But this is not necessarily due to the fact that the high-shear layer “rolls up” into the currently developing Ω and therefore disappears [1]. Thus, the nonlinear breakdown process to turbulence is not caused by a mere inflectional instability of the high-shear layer on top of the A -vortex, even if the shear layer visualization in figure 7 might suggest this, but is a much more complicated process involving several different mechanisms.

Further downstream, the amplification process of background disturbances becomes even more complex when the vortical structures and high-shear layers generated in different disturbance cycles start to interact. Starting at about $x = 800$ mm in figure 7(d), the Ω -vortices of a given disturbance cycle catch up with the structures generated one cycle before. The interaction of the Ω -vortices with the high-shear layer generated by the tail of the preceding A -vortex close to the wall, and with its legs, generates very strong shear that moves very quickly towards the wall (starting at $x \approx 810$ mm in figure 7(a)). The close-to-the-wall structures are modulated by the structures moving at the outer edge of the boundary layer. These modulations initiate the breakdown of the former into smaller ones. This accelerates the development towards fully turbulent flow. As an additional effect, the legs that connect the accelerated Ω -vortices with the tip of the A -vortex, or with the Ω next to them, are strongly stretched as they propel themselves towards the wall where the already existing high-shear layer is intensified (compare $x \approx 810$ mm in figure 6(a) and 7(a)).

Many new small vortical structures and high-shear layers appear in the following development through these interactions, which can be well observed comparing figures 6, 7 and 8. Looking at the latest figure, we can easily see why we need such a high resolution in our DNS: the boundary layer is filled with a lot of small-scale vortices compared to the wavelength of the original Tollmien-Schlichting disturbance which is $\lambda_{TS} \approx 43$ mm. This conglomeration of new structures is also very sensitive to background disturbances because of the complex interactions that occur between them. Most likely, the non-periodic motion from the upstream development as described earlier will be amplified and spread to the sides of the center plane ($z = 0$ mm) in this environment. Figure 8 also shows that the structures at the off-center position break down independently from those in the spanwise center. The generation and early development of these secondary structures can be observed in figure 6 at $z = \pm 12$ mm. Finally, a lot of symmetric, as well as asymmetric, structures develop during the late-stage transition process. The influence of asymmetric background perturbations at these very late stages of the transition process has been discussed in detail in [7] and [8].

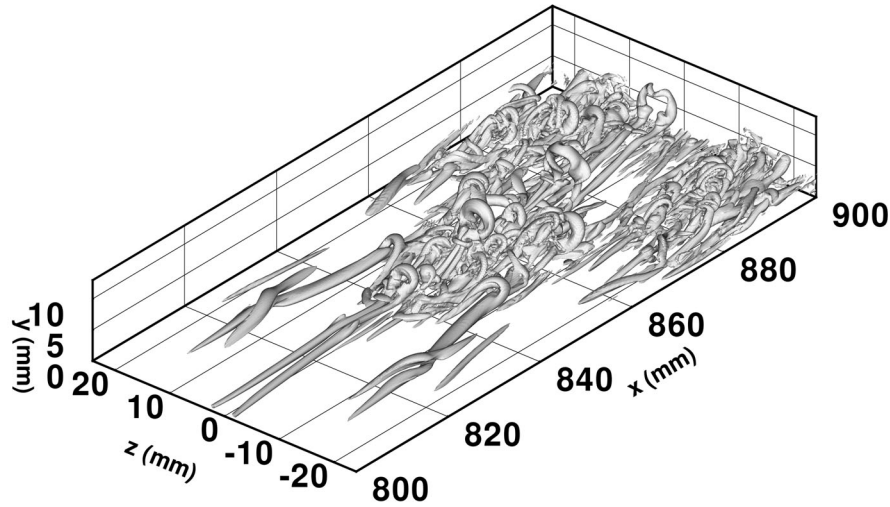


Fig. 8. Vortices in the later stage of the transition process at $t/T = 0.7$ downstream of the region shown in figure 6

4 Conclusions

The present picture of the randomization process seems to be fully confirmed by the experimental data in [1]. The inclined high-shear layer between the legs of the Λ -vortex exhibits increasing phase jitter (i.e. randomization) starting from its tip towards the wall region. In this process, the strongest instantaneous wall-normal shear $\partial U/\partial y$ occurs close to the wall below the Ω -loops and not in the high-shear layer that appears as a satellite on top of the Λ -vortex. Eventually, the regions of strong random velocity fluctuations in the layer closest to the wall enlarge, spread sideways and merge.

The direct numerical simulations provide the full unsteady, instantaneous flow field and are therefore extremely helpful for interpreting and understanding the results obtained by the measurements.

References

1. S. Bake, D. G. W. Meyer, and U. Rist. Turbulence mechanism in Klebanoff-transition. A quantitative comparison of experiment and direct numerical simulation. *J. Fluid Mech.*, 459:217–243, 2002.
2. V. I. Borodulin, V. R. Gaponenko, Y. S. Kachanov, D. G. W. Meyer, U. Rist, Q. X. Lian, and C. B. Lee. Late-stage transitional boundary-layer structures. Direct numerical simulation and experiment. *Theor. Comput. Fluid Dynamics*, 15(5):317–337, 2002.

3. C. Gmelin. *Numerische Untersuchungen zur aktiven Dämpfung von Störungen im Vorfeld der laminar-turbulenten Transition*. Dissertation, Universität Stuttgart, 2003.
4. C. Gmelin, U. Rist, M. Kloker, and S. Wagner. DNS of active control of disturbances in a Blasius boundary layer. In E. Krause and W. Jäger, editors, *High Performance Computing in Science and Engineering '01*, pages 273–285, Heidelberg, 2002. Springer.
5. M. Kloker. A robust high-resolution split-type compact FD-scheme for spatial direct numerical simulation of boundary-layer transition. *Appl. Sci. Research*, 59(4):353–377, 1998.
6. U. Maucher, U. Rist, M. Kloker, and S. Wagner. DNS of laminar-turbulent transition in separation bubbles. In E. Krause and W. Jäger, editors, *High Performance Computing in Science and Engineering '99*, pages 279–294, Heidelberg, 2000. Springer.
7. D. G. W. Meyer. *Direkte numerische Simulation nichtlinearer Transitionsmechanismen in der Strömungsgrenzschicht einer ebenen Platte*. Dissertation, Universität Stuttgart, 2003.
8. D. G. W. Meyer, U. Rist, and S. Wagner. Direct numerical simulation of the development of asymmetric perturbations at very late stages of the transition process. In S. Wagner, M. Kloker, and U. Rist, editors, *Recent Results in Laminar-Turbulent Transition – Selected Numerical and Experimental Contributions from the DFG-Verbundschwerpunktprogramm “Transition” in Germany*, NNFM, pages 213–222, Heidelberg, 2003. Springer.
9. P. Moin, A. Leonard, and J. Kim. Evolution of a curved vortex filament into a vortex ring. *Phys. Fluids*, 29(4):955–963, 1986.
10. S. A. Orszag. Numerical simulation of incompressible flows within simple boundaries. I. Galerkin (spectral) representations. *SIAM*, 1(4):293–327, 1971.
11. C. Stemmer, M. Kloker, U. Rist, and S. Wagner. DNS of point-source induced transition in an airfoil boundary-layer flow. In E. Krause and W. Jäger, editors, *High Performance Computing in Science and Engineering '98*, pages 213–222, Heidelberg, 1999. Springer.
12. S. Wagner, M. Kloker, and U. Rist, editors. *Recent Results in Laminar-Turbulent Transition – Selected Numerical and Experimental Contributions from the DFG-Verbundschwerpunktprogramm “Transition” in Germany*. NNFM, Springer, Heidelberg, 2003.
13. P. Wassermann and M. Kloker. Mechanisms and passive control of crossflow-vortex-induced transition in a three-dimensional boundary layer. *J. Fluid Mech.*, 456:49–84, 2002.
14. P. Wassermann, M. Kloker, U. Rist, and S. Wagner. DNS of laminar-turbulent transition in a 3-d aerodynamics boundary-layer flow. In E. Krause and W. Jäger, editors, *High Performance Computing in Science and Engineering 2000*, pages 275–289, Heidelberg, 2001. Springer.
15. A. Wörner. *Numerische Untersuchungen zum Entstehungsprozess von Grenzschichtstörungen durch die Interaktion von Schallwellen mit Oberflächenrauigkeiten*. Dissertation, Universität Stuttgart, 2003.
16. J. Zhou, R. J. Adrian, S. Balachandar, and T. M. Kendall. Mechanisms for generating coherent packets of hairpin vortices in channel flow. *J. Fluid Mech.*, 387:353–396, 1999.